In-plane photovoltage and photoluminescence studies in sequentially grown GaInNAs and GaInAs quantum wells

Article *in* Journal of Applied Physics · March 2003

DOI: 10.1063/1.1541104

CITATIONS
16

READS
63

11 authors, including:

Ali Teke
Balikesir University
38 PUBLICATIONS **8,885** CITATIONS

SEE PROFILE

M. C. Arikan
Istanbul University
69 PUBLICATIONS **939** CITATIONS

SEE PROFILE

Xavier Marie
Institut National des Sciences Appliquées de Toulouse
427 PUBLICATIONS **9,693** CITATIONS

SEE PROFILE

In-plane photovoltage and photoluminescence studies in sequentially grown GaInNAs and GaInAs quantum wells

S. Mazzucato and N. Balkan[a)]
Department of ESE, Photonics Group, University of Essex, CO4 3SQ, Colchester, United Kingdom

A. Teke
Department of ESE, Photonics Group, University of Essex, CO4 3SQ, United Kingdom and Department of Physics, Balikesir University, Balikesir, Turkey

A. Erol
Department of Physics, Istanbul University, Vezneciler, Istanbul, Turkey

R. J. Potter
Department of ESE, Photonics Group, University of Essex, CO4 3SQ, Colchester, United Kingdom

M. C. Arikan
Department of Physics, Istanbul University, Vezneciler, Istanbul, Turkey

X. Marie
Département de Physique, Laboratoire de Physique de la Matière Condensée, CNRS UMR 5830, INSA, Complex Scientifique de Rangueil, 31077 Toulouse cedex, France

C. Fontaine, H. Carrère, E. Bedel, and G. Lacoste
Laboratoire d'Analyse et d'Architecture des Systèmes (LAAS-CNRS), 7 avenue du Colonel Roche, 31077 Toulouse cedex 4, France

(Received 29 August 2002; accepted 9 December 2002)

We have investigated in-plane photovoltage (IPV) and photoluminescence (PL) in sequentially grown $Ga_{0.8}In_{0.2}As/GaAs$ and $Ga_{0.8}In_{0.2}N_{0.015}As_{0.985}/GaAs$ quantum wells. Temperature, excitation intensity, spectral and time dependent study of the IPV, arising from Fermi level fluctuations along the layers of the double quantum well structure, gives valuable information about the nonradiative centers and hence about the optical quality of the GaInNAs quantum well. It also provides information about the radiative transition energies in all the layers. In order to obtain either the trap activation energies and the detrapping rates of photogenerated carriers in the GaInNAs the IPV results are analyzed in terms of a theoretical model based on random doping fluctuations in nominally undoped multilayer structures. The PL results are analyzed in terms of the band anticrossing model to obtain the electron effective mass from the coupling parameter C_{NM}.
 [DOI: 10.1063/1.1541104]

I. INTRODUCTION

The quaternary alloys $Ga_xIn_{1-x}N_yAs_{1-y}$ (dilute nitrides) promise to be ideal material systems for applications in light emitting diodes, laser diodes, semiconductor optical amplifiers, switches, photodetectors, and wavelength converters operating in the 1.3–1.55 μm spectral range of optical communication systems. The introduction of a small amount of nitrogen (typically less than 5%) in GaInAs for band gap reduction was first proposed by Kondow *et al.*[1] Since then, it has been shown that laser diodes based on reduced-strain $Ga_xIn_{1-x}N_yAs_{1-y}/GaAs$ quantum wells have vastly improved characteristics and better temperature stability compared to InGaAsP/InP based devices.[2–4] $Ga_xIn_{1-x}N_yAs_{1-y}/GaAs$ structures are also attractive for applications in vertical-cavity surface-emitting lasers,[5] resonant cavity enhanced photodetectors,[6] and distributed feedback lasers.[7] This is because they allow the use of lattice matched, high refractive index contrast GaAs/AlAs distributed Bragg reflectors.

The difficulty of incorporating nitrogen into GaInAs while maintaining good optical quality has provoked much work to establish an understanding of the underlying factors determining the optical quality of GaInNAs, such as composition, growth, and annealing conditions.[8] Standard experimental techniques, such as photoluminescence (PL) spectroscopy, surface photovoltage spectroscopy (SPS), deep level transient spectroscopy and spectral photoconductivity[9–11] are commonly employed to investigate the presence of spatial and compositional nonuniformities, potential fluctuations, and radiative and nonradiative centers. In this work we used an experimental technique, the in-plane photovoltage (IPV) together with orthodox PL techniques to investigate the optical properties of as grown $Ga_xIn_{1-x}N_yAs_{1-y}/GaAs$ single quantum wells (SQWs) and compared the results with those obtained from a sequentially grown GaInAs/GaAs SQW.

When a $p-n$ junction is illuminated with light of appropriate wavelength a photovoltage (SPS) is created between

a)Author to whom correspondence should be addressed; electronic mail: balkan@essex.ac.uk

the p and the n contacts by the spatial separation of photogenerated carriers and then their subsequent movement to the top and the bottom sides of the device under the influence of the surface electric field. The SPS is therefore the open circuit voltage across the junction, measured capacitively, perpendicular to the layers.[10] However, the IPV is also predicted to occur in highly compensated material as a result of random potential fluctuations.[12] In the IPV technique two contacts are diffused through the layers of a multilayer structure (single or multiple QWs or a high electron mobility transistor structure). The open circuit IPV, which is recorded longitudinally between the two contacts, carriers the same spectral information as the absorption coefficient of the individual layers. The theory of the IPV was developed and the first experimental studies were reported on undoped GaAs/GaAlAs quantum well structures in the early. The results were explained in terms of effective $p-i$ and $n-i$ junctions randomly distributed along the layers.[13,14]

There has been only one reported study of spectral photovoltage in GaInNAs using the SPS technique.[11] No work to date has been reported concerning IPV in GaInNAs or other dilute nitrides. The aim of the current work is to investigate IPV in as grown $Ga_{0.8}In_{0.2}N_yAs_{1-y}/GaAs$ SQW as a function of photon energy, lattice temperature, modulation frequency, and excitation intensity. The IPV results, coupled with the PL measurements, are used to obtain the trap energies and detrapping time constants of photogenerated carriers in the GaInNAs, the parameters concerning the interaction strength between the localized nitrogen states and the host matrix state (GaInAs), and the electron effective mass in GaInNAs.

The article is organized as follows. In Sec. II the theory of in-plane photovoltage based on random doping fluctuations in the two-dimensional (2D) semiconductor material is revisited and the trapping dynamics are incorporated into the theoretical model. In Sec. III experimental results concerning the IPV and PL measurements are presented and discussed in terms of the BAC and random doping fluctuations.

II. THEORY

In order to explain our results concerning the spectral, transient and temperature dependent IPV we start with a theoretical model proposed by Ridley.[12] Here we modify the model to take into account the effect of differential trapping of excess carriers on the temperature and the illumination intensity dependence of the equilibrium IPV. In our calculations we also include the effect of trapping dynamics on the IPV transients. The model was originally developed for a GaAs/AlGaAs QW system and accounts for the effect of random doping fluctuations on the Fermi level in a fundamental volume whose dimensions are determined by the screening length. In the absence of fluctuations, the mean position of the Fermi level is entirely determined by the average concentration of donor and acceptor impurities. When the effect of fluctuations is strong, the material is effectively converted into a two-component system which is composed of intrinsic-n and intrinsic-p type regions. This effect gives rise to $n-i$ and/or $p-i$ junctions associated with an effective potential barrier randomly distributed within the material. These junctions produce photovoltages unrelated to contacts or to macroscopic impurity gradients when the sample is illuminated. These random fluctuations are originated by the presence of material nonuniformity inside the specimen. Sources of these nonuniformities can be doping fluctuations, as well as fluctuations on the layer widths or on the composition.[13] When the photogenerated minority carrier concentration is small simple expressions can be deduced for the photovoltage developing at a specific $n-i$ or $p-i$ junction by using standard theory.[14]

A. IPV in equilibrium in the absence of trapping

If the junction is illuminated by photons with energies $h\nu > E_g$, excess electron–hole pairs are created within a diffusion length on both sides of the $p-n$ junction. The number of electrons and holes created per second are proportional to L_eG and L_hG, respectively. G is the generation rate ($cm^{-3}\,s^{-1}$), and L_e and L_h are the diffusion length for electrons and holes, respectively. Thus, the total photogenerated current density J_{ph}, due to the diffusion of these carriers across the junction, is given by

$$J_{ph} = eG(L_h + L_e). \tag{1}$$

Therefore, the total current density for the illuminated diode is equal to

$$J = e\left(\frac{L_h}{\tau_h}p_{n0} + \frac{L_e}{\tau_e}n_{p0}\right)\left[\exp\left(\frac{eV_{bi}}{k_BT}\right) - 1\right] - eG(L_h + L_e) \tag{2}$$

V_{bi} being the built-in potential, and τ_h and τ_e the mean life of excess electron–hole pairs in the n and in the p side, respectively. Finally p_{n0} is the hole concentration in the n-type material, and n_{p0} is the electron concentration in the p type. The negative sign in the second term arises because the photogenerated current (from n side to p side) is opposed to the main diode current (from p side to n side). For the open-circuited diode, $J = 0$, the in-plane photovoltage developed at a temperature T is given by

$$\mathrm{IPV} = \frac{k_BT}{e}\ln\left(\frac{J_{p_n} + J_{n_p}}{J_{p_{n0}} + J_{n_{p0}}}\right), \tag{3}$$

where J_{p_n} and J_{n_p} are the hole and electron diffusion current densities under illumination, and $J_{p_{n0}}$ and $J_{n_{p0}}$ are the hole and electron diffusion current densities in dark in the n- and p-type region, respectively. Since Eq. (3) is a standard expression for a $p-n$ homojunction, it can be easily adopted to an $n-i$ and/or $p-i$ junction.

By considering a $n-i$ type junction ($J_{p_{n0}} \ll J_{n_{p0}}$), the photovoltage is given by

$$\mathrm{IPV} = \frac{k_BT}{e}\ln\left(\frac{J_{p_n} + J_{n_p}}{J_{n_{p0}}}\right). \tag{4}$$

In the intrinsic region, we can write the current densities in terms of the electron density in darkness n_{p0} and the equilibrium excess electron density under illumination Δn_0 as

$$\frac{J_{n_p}}{J_{n_{p0}}}=\frac{n_{p0}+\Delta n_0}{n_{p0}}=1+\frac{\Delta n_0}{n_{p0}}. \tag{5}$$

By substituting this expression into Eq. (4) we obtain

$$\mathrm{IPV}=\frac{k_BT}{e}\ln\left(1+\frac{\Delta n_0}{n_{p0}}+\frac{J_{p_n}}{J_{n_{p0}}}\right). \tag{6}$$

For the $n-i$ junction it can be assumed that $J_{n_{p0}}\gg J_{p_n}$ in the linear region, so that

$$\mathrm{IPV}=\frac{k_BT}{e}\ln\left(1+\frac{\Delta n_0}{n_{p0}}\right)\approx\frac{k_BT}{e}\frac{\Delta n_0}{n_{p0}}. \tag{7}$$

The electron density on either side of the barrier is given by

$$n_{n0}=N_C\exp\left[-\left(\frac{E_C-E_{F_n}}{k_BT}\right)\right]$$

and

$$n_{p0}=N_C\exp\left[-\left(\frac{E_C-E_{F_p}}{k_BT}\right)\right], \tag{8}$$

where N_C is the density of state in the conduction band and E_C is the conduction band energy. E_{F_n} and E_{F_p} are the Fermi energies in the *n*-type and intrinsic regions, respectively. Therefore

$$n_{p0}=n_{n0}\exp\left[-\left(\frac{E_{F_n}-E_{F_p}}{k_BT}\right)\right]. \tag{9}$$

Substituting for n_{p0} in Eq. (7), the photovoltage developed at the barrier is given by

$$\begin{aligned}\mathrm{IPV}&=\frac{k_BT}{e}\frac{\Delta n_0}{n_{n0}}\exp\left(\frac{\phi}{k_BT}\right)\\&=\frac{k_BT}{en_{n0}}\frac{\eta\alpha(\lambda)I}{h\nu}\tau\exp\left(\frac{\phi}{k_BT}\right)=\frac{k_BT}{e}\frac{cI}{n_{n0}}\exp\left(\frac{\phi}{k_BT}\right),\end{aligned} \tag{10}$$

where $\phi=E_{F_n}-E_{F_p}$ and

$$\Delta n_0=\frac{\eta\alpha(\lambda)I}{h\nu}\tau,\quad \Delta n_0=cI\ (c\ \text{is a constant}), \tag{11}$$

where η, $\alpha(\lambda)$, I, $h\nu$, and τ are the quantum efficiency, wavelength dependent absorption coefficient, intensity of the incident photons, photon energy, and the excess carrier lifetime, respectively.

In the derivation of the expressions above, it is assumed that the sample thickness d satisfies the following conditions: $d\gg\lambda$, therefore the inference effects due to inner reflections are negligible; and the sample is thin enough so that the excess carriers are generated uniformly throughout the sample ($\alpha d\ll 1$).

Also, the surface recombination is neglected and the number of traps is assumed to be negligible or there is no differential trapping of electrons and holes, therefore excess electron and hole densities at any given time are equal: $\Delta n=\Delta p$. Furthermore the light intensity is assumed to be low enough to justify $\Delta n_0\ll n_{n0}$ so that the excess carrier lifetime τ is constant.

According to Eq. (10) the in-plane photovoltage carriers the same spectral information as the absorption coefficient $\alpha(\lambda)$ and varies linearly with the photon intensity. For large values of excess carrier densities at high excitation intensities the variation of Δn_0 with I will depend on the recombination law. In the case of radiative recombination at very high excitation intensities ($\Delta n,\ \Delta p\gg n_{n0},\ p_{p0}$, for example), it results that $\Delta n_0\propto\sqrt{I}$.

For a $p-i$ barrier an expression similar to Eq. (10) is also obtained

$$\mathrm{IPV}=-\frac{k_BT}{e}\frac{cI}{p_{p0}}\exp\left(\frac{\phi}{k_BT}\right), \tag{12}$$

where p_{p0} is the hole density in the *p* side of the barrier.

According to Eqs. (10) and (12) at a fixed temperature the IPV measured as a function of the incident photon energy (spectral IPV) should provide information about the intersubband and impurity transitions. Furthermore at a fixed illumination intensity, a plot of the logarithm of (IPV/T) against $1/T$ should give a straight line with a slope ϕ/k_B. In reality, however, because of the randomness of the doping fluctuations the ϕ value can take any random value between $\phi_{\max}$ and $\phi_{\min}$. Therefore, the $\log(\mathrm{IPV}/T)$ versus $1/T$ plot will not be a straight line with a single slope but a curve with a temperature dependent slope.

B. Transient IPV in the absence of trapping

If the illumination is turned off after the steady state condition is established at $t=0$, the equilibrium excess electron density will decay as

$$\Delta n=\Delta n_0\exp\left(-\frac{t}{\tau}\right). \tag{13}$$

Therefore the time dependent IPV signal will be

$$(\mathrm{IPV})_{\text{transient}}=[\mathrm{IPV}]\exp\left(-\frac{t}{\tau}\right), \tag{14}$$

where [IPV] corresponds to the equilibrium condition as in Eq. (10). According to Eq. (14) the decay of the IPV can be used to obtain the excess carrier lifetime (recombination time constant) τ. If the illumination is switched on at $t=0$ and held constant from $t=0$ to $t=t_0$ and switched off at $t=t_0$ before the steady state is achieved then[15]

$$\begin{aligned}&\Delta n=\Delta n_0\left[1-\exp\left(-\frac{t}{\tau}\right)\right]\quad(0\leqslant t\leqslant t_0),\\&\Delta n=\Delta n_0\left[1-\exp\left(-\frac{t}{\tau}\right)\right]\exp\left[-\frac{(t-t_0)}{\tau}\right]\quad(t\geqslant t_0),\end{aligned} \tag{15}$$

and the time dependent IPV signal is

$$(\mathrm{IPV})_{\text{transient}}=[\mathrm{IPV}]\left[1-\exp\left(-\frac{t}{\tau}\right)\right]\exp\left[-\frac{(t-t_0)}{\tau}\right](t\geqslant t_0). \tag{16}$$

C. IPV in equilibrium in the presence of trapping

The theoretical model above assumes that the trap density is negligible. However, if the material contains safe traps in which differential trapping of either only electrons or only holes occurs in contrast to recombination traps where both excess electrons and holes are captured to recombine, then Eqs. (10)–(16) have to be modified to include the trap dynamics.

Following the notation in Ref. 16 we consider hole trapping first. The rate of change of excess hole density Δp is given by

$$\frac{d\Delta p}{dt}=\mathcal{R}-\frac{\Delta p}{\tau}-\frac{\Delta p}{\tau_1}+\frac{\Delta N_s}{\tau_2}, \tag{17}$$

where $\mathcal{R}$, τ, τ_1, τ_2, and ΔN_s are excess carrier generation rate $[\mathcal{R}=(\eta\alpha(\lambda)I/h\nu)]$, excess carrier lifetime in the absence of trapping, average lifetime of a hole before it is captured by a trap, mean time a hole spends in a safe trap before being re-excited to the valance band, and the excess hole concentration in the safe traps.

The rate of change of the holes in the safe trap is given by

$$\frac{d\Delta N_s}{dt}=\frac{\Delta p}{\tau_1}-\frac{\Delta N_s}{\tau_2}. \tag{18}$$

In equilibrium this leads to

$$\Delta N_{so}=\left[\frac{\tau_2}{\tau_1}\right]\Delta p_0. \tag{19}$$

Using Eqs. (17) and (19) we obtain the hole density

$$\Delta p_0=\mathcal{R}\tau.$$

The equilibrium hole density Δp_0 is not affected by trapping as expected. From the space charge neutrality $\Delta n=\Delta p+\Delta N_s$ so that in equilibrium we have from Eq. (19) the excess electron density as a function of τ_1 and τ_2

$$\Delta n_0=\Delta p_0\left[1+\left(\frac{\tau_2}{\tau_1}\right)\right]. \tag{20}$$

For $\tau_2>\tau_1$ the traps will increase the density of equilibrium excess electrons substantially and Δn can be approximated to

$$\Delta n_0\approx\Delta p_0\left(\frac{\tau_2}{\tau_1}\right)\approx\Delta N_s. \tag{21}$$

According to Eqs. (10) and (21) the increase in the equilibrium electron density will cause a considerable IPV to develop.

We now wish to relate IPV to the detrapping rate ($\nu=\tau_2^{-1}$), which is given by Kremer[17] as

$$\nu_2=A\exp\left(\frac{-E_{th}}{k_BT}\right), \tag{22}$$

where E_{th} is the energy difference between the hole trap and the valence band (trap emission energy) and A is a constant.

If we substitute Eqs. (21) and (22) into Eq. (10) we get

$$\mathrm{IPV}=\frac{k_BT\Delta p_0}{Aen_{n0}\tau_1}\exp\left(\frac{E_{th}+\phi}{k_BT}\right) \quad \text{for hole trapping.} \tag{23}$$

Therefore a plot of $\log(\mathrm{IPV}/T)$ versus $1/(k_BT)$ should give a straight line with a slope $(E_{th}+\phi)$. For deep traps when $E_{th}>\phi$ the slope will be equal to the trap emission energy. However, if there is more than one hole trap level present IPV will have a more complicated temperature dependence than that predicted by Eq. (23).

We can obtain the in-plane photovoltage in Eq. (12) for the case of electron trapping using similar equations to Eqs. (17)–(22)

$$\mathrm{IPV}=-\frac{k_BT\Delta n_0}{Aep_{p0}\tau_1}\exp\left(\frac{E_{te}+\phi}{k_BT}\right) \quad \text{for electron trapping.} \tag{24}$$

Here τ_1 and E_{te} are the electron trapping time constants and emission energy of the electron trap, respectively.

If both electron and hole traps are present, the relative values of E_{th} and E_{te} will determine whether Eq. (23) or (24) dominates the slope of the $\log(\mathrm{IPV}/T)$ versus $1/(k_BT)$ within a certain temperature range.

D. Transient IPV in the presence of traps

In the case of hole trapping when $\tau_2\gg\tau_1$ and $\tau_2\gg\tau$, if the illumination is turned off after the steady state has been established, according to Eqs. (18)–(20), the hole concentration will drop rapidly with the fast recombination time constant τ

$$\frac{d\Delta p}{dt}=-\frac{\Delta p}{\tau}$$

and

$$\frac{\Delta p}{\tau_1}=\frac{\Delta N_s}{\tau_2}. \tag{25}$$

After this fast initial drop, we have from Eq. (18)

$$\frac{d\Delta N_s}{dt}=-\frac{\Delta N}{\tau_2} \tag{26}$$

and then $\Delta N_s=\Delta N_{so}\exp(t/\tau)$ decreases with time constant τ_2.

From Eq. (21) when $\tau_2\gg\tau_1$ the density of excess electrons is

$$\Delta n\approx\Delta N_s. \tag{27}$$

Therefore using Eqs. (26) and (27) in Eq. (10) we obtain

$$(\mathrm{IPV})_{\mathrm{transient}}=[\mathrm{IPV}]\exp\left(-\frac{t}{\tau_2}\right), \tag{28}$$

where $[\mathrm{IPV}]$ is the equilibrium IPV in Eq. (23) for hole trapping, or that in Eq. (24) for electron trapping. The result in Eq. (28) indicates that after the initial decay associated with the fast recombination time constant, the IPV transients can be used to obtain the detrapping time constant τ_2 (see Fig. 1).

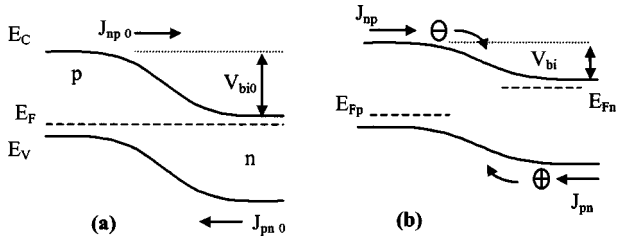

FIG. 1. Schematic diagram of a $p-n$ junction (a) in darkness and (b) under illumination. V_{bi0} is the built-in voltage in darkness, V_{bi} is the one when the sample is illuminated. The other symbols are explained.

III. EXPERIMENTAL RESULTS AND DISCUSSION

The sample used in this work was grown on a semi-insulating (100) GaAs substrate by molecular beam epitaxy in a RIBER 2300 chamber. Ultrahigh-purity N_2 was injected through a rf nitrogen radical beam source (Oxford Applied Research HD25R) operated at 13.56 MHz to generate active N species. The sample, code numbered E#752b1, has a double QW (DQW) structure. The first well is $Ga_{0.8}In_{0.2}As$ and the second $Ga_{0.8}In_{0.2}N_yAs_{1-y}$, each 90 Å wide as shown in Fig. 2. The substrate temperature was 480 °C during the growth of both QWs and the growth rate was 0.6 μm/h. GaAs layers were grown at 600 °C with a growth rate of 0.7 μm/h. N_2 flow rate was 0.01 sccm and rf power was 200 W. The N content was determined by secondary ion mass spectrometry analysis of bulk GaNAs that was grown in the same conditions as the QW. The layers were analyzed using a Cs+ primary ion beam and positive secondary ions configuration in order to minimize the matrix effects. From this calibration, we estimate the nitrogen content in the alloy, $y(\mathrm{N})=1.5\% \pm 0.2\%$.

The sample was fabricated in the form of simple bar. Ohmic contacts were formed by diffusing Au/AuGe/Ni/Au for 120 s at an anneal temperature of $T=420$ °C. An area of 1 mm^2 between the contacts was available for the top illumination of the sample in the photovoltage measurements.

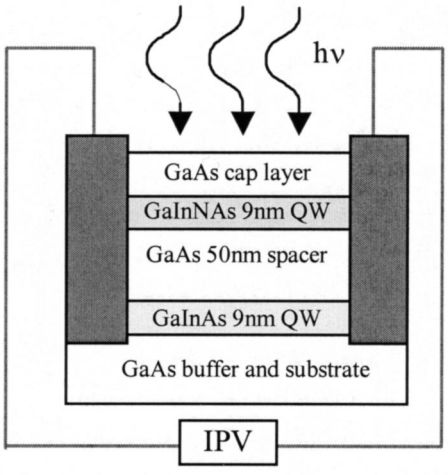

FIG. 2. Schematic diagram of the sample structure. Top incident light and external electrical circuit are also shown.

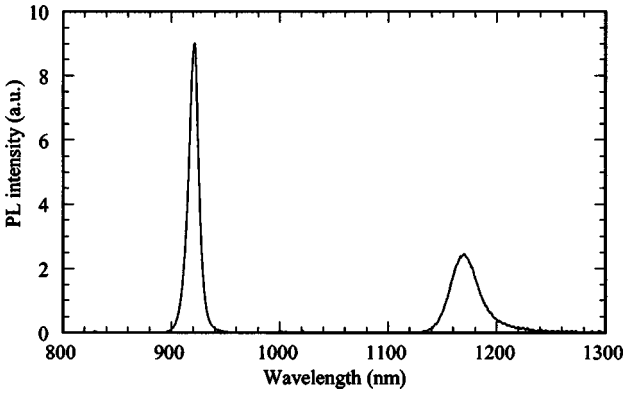

FIG. 3. Photoluminescence spectrum taken at $T=2$ K. The intensity scale is magnified by $\times 80$ above 1000 nm.

A. Photoluminescence

In order to determine the effective band gaps of the GaInNAs and GaInAs QWs we carried out PL measurements at temperatures between $T=2$ and 300 K. The 647 nm line of a cw krypton ion laser was used as the excitation source. The beam was chopped and focused onto the sample defining a spot size of diameter ~0.25 mm. A boxcar averager in conjunction with a 1/3 m monochromator and a cooled Hamamatsu InP/GaInAs near infrared photomultiplier were used to disperse and detect the luminescence.

A typical PL spectrum taken at 2 K is shown in Fig. 3. The intensity scale is split at 1000 nm so that both peaks are visible on the same axis. The addition of nitrogen reduces the PL intensity and shifts the peak wavelength to longer wavelengths, in common with other observations in the literature. PL efficiency is often improved by rapid thermal annealing.[8] However, in this study both the PL and the IPV are reported in as grown samples only.

Figure 4 shows the temperature dependence of the PL peak wavelength for GaInAs and GaInNAs. At low temperatures, the GaInAs peak has very weak temperature dependence. At $T>40$ K, however, the peak wavelength increases, initially, nonlinearly but becomes more linear at high temperatures. The behavior of the GaInNAs peak at low tem-

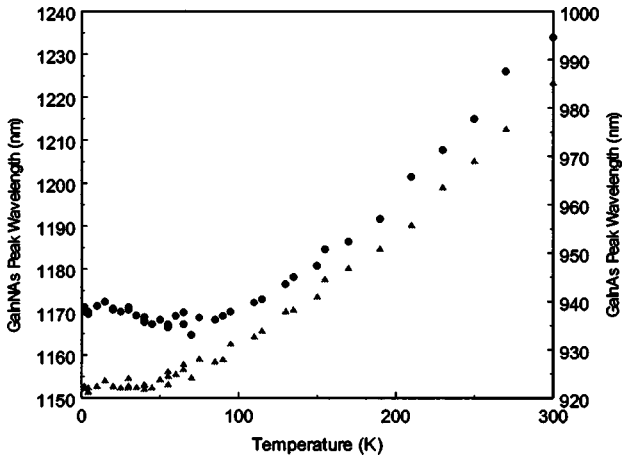

FIG. 4. Temperature dependence of ( ) GaInAs and ( ) GaInNAs PL peak wavelengths.

peratures ($T<30$ K) is similar to GaInAs where no measurable change in the peak wavelength is observed. Unlike the GaInAs PL, however, the peak wavelength of the GaInNAs PL decreases with increasing temperature between $T=30$ and 70 K, instead of increasing as would be expected from band gap shrinkage. The net decrease in the peak wavelength is around 12 nm corresponding to an increase in energy of 12 meV. Anomalous temperature dependence of PL energy similar to our observation has been reported in GaInNAs and in ternary nitrides, and referred to as 'S-shape' dependence.[18–20] It is often explained in terms of exciton localization at potential fluctuations induced by the presence of nitrogen, which may arise as a result of well width and composition fluctuations or strain.[18] Their existence is further supported by our observation of large photovoltages developing in the plane of the layers as discussed below. As a result of the randomness of such variations the values reported in the literature for the magnitude of the energy shift and the temperature range where this occurs varies significantly. If the observed shift of 12 meV in our sample is solely due to well width fluctuations it corresponds to a well-width variation of $\Delta L_z=3-4$ monolayers.

The electron effective mass (m_e^*) in dilute nitrides and its dependence upon composition has been investigated experimentally and theoretically by a number of groups. Most theoretical[21–23] and experimental[10,24–26] results agree that the incorporation of nitrogen into GaAs or GaInAs increases m_e^* greatly. However, there is very little agreement between the values quoted in the literature by different groups. Most experimental values of m_e^* have been obtained using indirect methods such as through the analysis of the carrier confinement energies.[10,24,26] Such measurements rely upon certain assumptions and approximations. In addition the possibility of unintentional doping of material, which will effect the value of m_e^*,[22] is often overlooked. Direct measurements of m_e^* using cyclotron resonance has been limited to GaNAs with very low nitrogen concentration.[25] As far as we are aware no direct measurements of m_e^* in GaInNAs have been reported. In this work we used the band anticrossing model to estimate m_e^* in our material given by[21]

$$m_e^*=m^*_{(\mathrm{GaInAs})}\left[1+\left(\frac{V_{\mathrm{MN}}}{E_{\mathrm{N}}-E}\right)^2\right], \tag{29}$$

where E is the electron energy relative to the valence band edge, $m^*_{(\mathrm{GaInAs})}$ is the electron effective mass in the N free alloy ($m^*(\mathrm{Ga}_x\mathrm{In}_{1-x}\mathrm{As})=0.026+0.041x$),[27] E_{N} is the localized nitrogen state energy (relative to the top of the valence band) and V_{MN} is the matrix element describing the interaction between the two states. ($V_{\mathrm{MN}}=C_{\mathrm{NM}}\sqrt{y}$,[28] where C_{NM} is a constant and y is the nitrogen fraction).

We have determined the values of C_{NM} from the temperature dependence of the GaInNAs peak wavelength as described by us elsewhere.[8] In these calculations we took $C_{\mathrm{NM}}=3.17$ for 20% indium and $E_{\mathrm{N}}=1.57$ for the same sample as the one used in the current work. In the calculations we took into account the effects of both nitrogen and indium fraction. Using these values for E_{N}, C_{NM}, and y we get an electron effective mass of $m_e^*=0.0782m_0$. This value compares well with the results reported by Pan *et al.*[10] for GaInNAs with 30% indium concentration and 1% nitrogen.

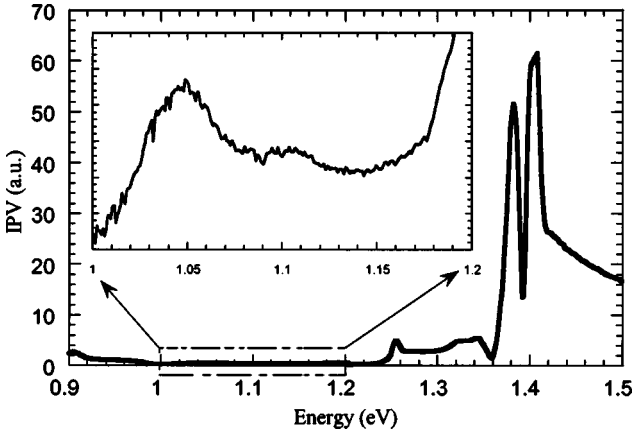

FIG. 5. IPV spectrum at room temperature. The inset shows the 1.0–1.2 eV region with a higher resolution.

B. Spectral IPV

Spectral IPV measurements were carried out using a closed-cycle refrigerator at temperatures between $T=27$ and 300 K, and in the spectral range between $\lambda=0.8$ and 1.55 μm. The broadband emission from a quartz halogen lamp was used as the excitation source. It was dispersed with a 1/2 m monochromator and chopped with a mechanical chopper defining a repetition time of 0.8 s and a pulse width of 20 ms. Figure 5 shows a typical IPV spectrum, taken at $T=300$ K. The spectrum is normalized with respect to the spectral output of the halogen lamp. The inset of Fig. 5 shows the IPV spectrum in the 1.0–1.2 μm wavelength range with a higher resolution. The high energy peaks at $h\nu=1.41$ and 1.39 eV are due to band-to-band and $e-A$ (carbon) transitions in GaAs, respectively. IPV measurements give a clear indication of the optical quality of the specimen. In a perfect material with no doping or potential fluctuations, the IPV is not expected to develop along the layers of the device. The high intensity IPV observed in the spectral region corresponding to the GaAs transitions indicates the presence of large potential fluctuations in this layer. Subsequent transmission electron microscope (TEM) study on the same specimen is shown in Fig. 6, confirming the presence of a large number of dislocations and nonuniform impurities in the GaAs capping layer in accord with the spectral IPV results.

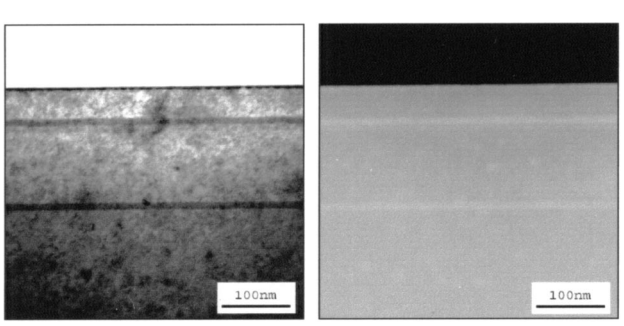

FIG. 6. The bright and dark field TEM images of the sample.

The photovoltage due to GaInAs QW excitations is in the spectral range between $h\nu = 1.26$ and 1.35 eV, where the low energy peak at $h\nu = 1.26$ eV ($\lambda = 0.87\ \mu$m) corresponds to the $e1-$hh1 transition and agrees well with the PL peak wavelength in Fig. 4. The broad higher energy peaks at 1.32 and 1.35 eV are due to the higher subband transitions in GaInAs.

GaInNAs QW transitions are situated at $h\nu < 1.15$ eV, with a broadband below 1.24 μm (1 eV) corresponding to $e1-$hh1 transitions, which are broadened due to potential fluctuations and hence due to the localization of the tail states. Two broad peaks close to $\lambda = 1.18\ \mu$m (1.05 eV) and 1.13 μm (1.1 eV) are probably associated with the higher energy transitions in the GaInNAs QW. It is worth noting that the magnitude of the IPV associated with the spectral region corresponding to the GaInNAs QW transitions is much smaller than those for both GaAs and GaInAs QW. This indicates that GaInNAs has a very good optical quality for an unannealed, as grown material. This is also confirmed from the spectral PL measurements in Fig. 3 where the GaInNAs emission has only 41 meV full width half maximum. With the nominal parameters of the GaInNAs QW (20% In, 1.5% N, 9 nm thickness), a theoretical approach gives the following values for the previous transitions: $e1-$hh1:0.976 eV; $e1-1$h1:1.046 eV; and $e2-$hh2:1.088 eV. These last two values are quite close to the transition observed in the inset of Fig. 5, with the $e1-1$h1 transition stronger than $e2-$hh2. The same behavior had been reported in the Pan *et al.* paper.[10]

C. Excitation intensity dependence of IPV

IPV measurements as a function of excitation intensity were also carried out between 120 and 320 K. In the experiments the use of the 1.064 μm line of a cw Nd:YAG laser the excitation source ensured absorption in the GaInNAs QW only. Therefore, the IPV recorded was due to GaInNAs transitions only. The incident beam on the sample was slightly defocused so that the laser spot covered the whole exposed area of the sample ensuring a uniform illumination. The incident laser power was varied between 20 and 620 mW using a set of calibrated neutral density filters. The steady state open circuit voltage V_{OC} between the contacts was measured using a Keithley177 Microvolt DMM voltmeter. The setup was slightly modified to investigate the IPV in a quasisteady state regime, by modulating the laser beam with a mechanical chopper at different frequencies and recording the signal with a lock-in amplifier set in differential mode.

Figure 7 shows the excitation intensity dependence of IPV at room temperature. At low excitation intensities the IPV signal increases linearly with the excitation intensity as predicted by Eq. (10) of the theoretical model. When the power is increased above 100 mW, the signal increases less rapidly and has a square root dependence on intensity (IPV $\propto \sqrt{I}$) between 100 and 200 mW, as expected from the model for high excess carrier densities. The IPV signal saturates at excitation powers greater than 2000 mW. The reason for this saturation may be due to the dramatic reduction in the excess carrier lifetimes. This may occur because at such high excitation intensities the wave functions of the photogenerated carriers, confined to 2D GaInNAs overlap very strongly.[29] Another possibility is the band filling when the material becomes transparent to the incident radiation at such high excitation intensities.[30]

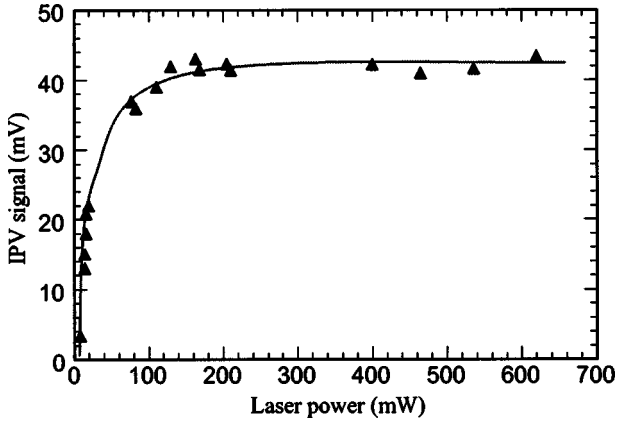

FIG. 7. Dependence of the IPV amplitude on excitation power for steady state at room temperature. The line is added to guide the eye.

D. Temperature dependence of IPV

IPV measurements as a function of temperature were carried out in the steady state between 120 and 320 K, by using the 1.064 μm line of a cw Nd:YAG laser. Temperature dependence of IPV is shown in the inset of Fig. 8. The measurements were made at a fixed laser power of 230 mW. It is clear that the temperature dependence of the IPV has three distinct regions. In the high temperature region between 250 and 320 K the IPV signal increases rapidly with decreasing temperature. In the region between 250 and 200 K the rate of increase of the IPV signal with decreasing temperature is much reduced. In the low temperature region ($T < 200$ K) once more the signal increases rapidly.

In order to analyze temperature dependence of the IPV, we plotted the logarithm of (IPV/T) as a function of $1/T$ as shown in Fig. 8. It is clear from the figure that in the lower

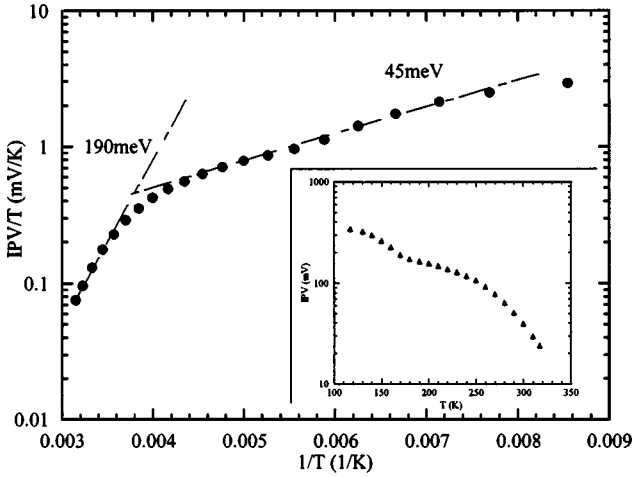

FIG. 8. IPV/T signal as a function of inverse temperature recorded in the steady state case with the incident laser power of 230 mW. The inset shows the three regions composing the temperature dependence of the IPV signal.

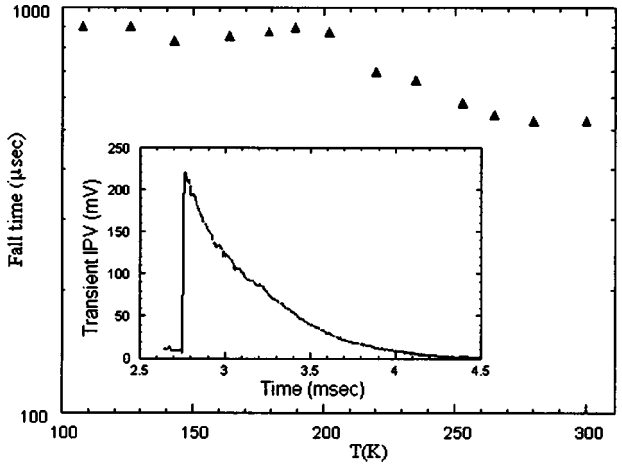

FIG. 9. Temperature dependence of fall time in transient IPV. In the inset a typical exponential decay of IPV recorded $T=108$ K is shown.

and the higher temperature regions log(IPV/T) has a thermally activated behavior as predicted by the theory. At temperatures $T>250$ K the activation energy is 190 meV. In the lower temperature region ($T<200$ K), however, the activation energy is 45 meV. In the transition region between 200 and 250 K there is no single activation energy.

The determination of the activation energies from the temperature dependence of the IPV, by itself, cannot provide information about whether these are related to the Fermi level separation ϕ in Eq. (10) for the case of IPV in the absence of trapping, or they represent the $E_{\text{th}}+\phi$ in Eq. (23) for the case of IPV in the presence of trapping. However, because the Fermi level fluctuations in the nominally undoped material are expected to have a random distribution between $\phi_{\max}$ and $\phi_{\min}$ values corresponding to the largest and the smallest potential barriers in the structure are due to the random doping fluctuations. Therefore the log(IPV/T) versus $1/T$ plot cannot be a straight line with a single slope but a curve with a temperature dependent slope. This is unlike our observations in Fig. 8. The observed activation energies correspond to $E_{\text{th}}+\phi$ in Eq. (23) or $E_{\text{te}}+\phi$ in Eq. (24) with $E_{\text{th},e}\gg\phi$. They are therefore the emission energies of two distinct traps in GaInNAs. Other groups, using different techniques, have found some traps in GaInNAs with similar activation energies.[31,32] Further evidence for the activation energies being representative of traps comes from the observation of the decay time constants of the IPV transients.

E. IPV transients

We studied the IPV transients by using a Q-switched, mode locked Nd:YAG laser at 1.064 μm wavelength as the excitation source. Light pulses of 100 ps width with 5 Hz repetition rate were applied to the sample, which was mounted on a high-speed inset in a liquid nitrogen cryostat. The measurement temperature range was between 108 and 300 K. An open-circuit transient IPV signal was recorded using a 300 MHz bandwidth digitizing oscilloscope. The IPV response of the sample to the laser pulse recorder at $T=108$ K is shown in the inset of Fig. 9. The temperature dependence of the fall time of the IPV signal is also shown in the figure. It is clear that there are also two distinct regimes for the decay time constants. At temperatures $T<200$ K it is close to 1 ms. In the high temperature region ($T>250$ K) it is in the 500 μs range. If we compare the IPV decay time constants with those in the expressions for the trap free case, i.e., Eq. (13)–(16), we see that the measured decay time constants of the signals are much longer than the excess carrier lifetimes, which are predicted to dominate the IPV transients. If we use Eq. (28), however, we see that the measured long decay time constants correspond to τ_2 in Eq. (28), which is the detrapping time of excess carriers and $\tau_2\gg\tau$. The traps have two distinct levels with emission energies, 45 and 190 meV, and associated detrapping time constants in the 1.0 and 0.5 ms ranges, respectively.

IV. CONCLUSIONS

We have investigated IPV and PL in sequentially grown $Ga_{0.8}In_{0.2}As/GaAs$ and $Ga_{0.8}In_{0.2}N_{0.015}As_{0.985}/GaAs$ quantum wells. Temperature, excitation intensity, spectral and time dependent study of the IPV, arising from Fermi level fluctuations along the layers of the DQW structure, have been shown to give valuable information about the nonradiative centers and hence about the optical quality of the GaInNAs QW. It also provides information about the radiative transition energies in all the layers. We have developed a model to explain the role of traps in the IPV dynamics, where the expressions have been derived for trap emission energies and detrapping rates of photogenerated carriers as well as the spectral and excitation intensity dependence of the IPV. We analyzed our experimental results in terms of a theoretical model to show the presence of two distinct traps in GaInNAs. The PL results are analyzed in terms of the band anticrossing model to obtain the electron effective mass from the coupling parameter C_{NM}. We find an electron effective mass of $m_e^*=0.0782\,m_0$.

ACKNOWLEDGMENTS

The authors are grateful to EPSRC for supporting the project (Grant Nos. GR/N08094 and GR/N07813). This work is also supported by French Ministry of Research: RNRT program (SINTROP's project) and CNRS program (Telecommunication project). A.T. would like to thank TUBITAK for their financial support (Grant No. NATO-B2) as a research fellow during his stay at Essex. The authors acknowledge Dr. P. Chalker and his group at the University of Liverpool for taking the TEM images of the sample.

[1] M. Kondow, K. Uomi, A. Niwa, T. Kitatani, S. Watahiki, and Y. Yazawa, Jpn. J. Appl. Phys., Part 1 **35**, 1273 (1996).
[2] T. Miyamoto, K. Takeuchi, T. Kageyama, F. Koyama, and K. Iga, J. Cryst. Growth **197**, 67 (1999).
[3] W. Shan, W. Walukiewicz, J. W. Ager, III, E. E. Haller, J. F. Geisz, D. J. Friedman, J. M. Olson, and S. R. Kurtz, J. Appl. Phys. **86**, 2349 (1999).
[4] H. P. Xin, K. L. Kavanagh, Z. Q. Zhu, and C. W. Tu, Appl. Phys. Lett. **74**, 2337 (1999).
[5] A. Wagner, C. Ellmers, F. Höhnsdorf, J. Koch, C. Agert, S. Leu, M. Hofmann, W. Stolz, and W. W. Rühle, Appl. Phys. Lett. **76**, 271 (2000).
[6] J. B. Héroux, X. Yàng, and W. I. Wang, Appl. Phys. Lett. **75**, 2716 (1999).
[7] M. Reinhardt, M. Fischer, M. Kamp, J. Hofmann, and A. Forchel, IEEE Photonics Technol. Lett. **12**, 239 (2000).
[8] R. J. Potter, S. Mazzucato, N. Balkan, M. J. Adams, P. R. Chalker, T. B.

Joyce, and T. J. Bullough, Superlattices Microstruct. **29**, 169 (2001).
[9] R. J. Potter, N. Balkan, X. Marie, H. Carrere, E. Bedel, and G. Lacoste, Phys. Status Solidi A **187**, 623 (2001).
[10] Z. Pan, L. H. Li, Y. W. Lin, B. Q. Sun, D. S. Jiang, and W. K. Ge, Appl. Phys. Lett. **78**, 2217 (2001).
[11] D. Kwon, R. J. Kaplar, S. A. Ringel, A. A. Allerman, S. R. Kurtz, and E. D. Jones, Appl. Phys. Lett. **74**, 2830 (1999).
[12] B. K. Ridley, Semicond. Sci. Technol. **3**, 286 (1988).
[13] M. E. Daniels, P. J. Bishop, and B. K. Ridley, Semicond. Sci. Technol. **3**, 1094 (1988).
[14] P. Bhattacharya, *Semiconductor Optoelectronic Devices* (Prentice Hall, Englewood, NJ 1997).
[15] B. K. Ridley, *Quantum Processes in Semiconductors*, 3rd ed. (Clarendon Press, Oxford, 1993).
[16] R. A. Smith, *Semiconductors* (Cambridge University Press, Cambridge, 1978).
[17] R. E. Kremer, M. C. Arikan, J. C. Abele, and J. S. Blakemore, J. Appl. Phys. **62**, 2424 (1987).
[18] L. Grenouillet, C. Bru-Chevallier, G. Guillot, P. Gilet, P. Duvaut, C. Vannuffel, A. Million, and A. Chenevas-Paule, Appl. Phys. Lett. **76**, 2241 (2000).
[19] A. Kaschner, T. Lüttgert, H. Born, A. Hoffmann, A. Yu. Egorov, and H. Riechert, Appl. Phys. Lett. **78**, 1391 (2001).
[20] I. A. Buyanova, W. M. Chen, G. Pozina, J. P. Bergman, B. Monemar, H. P. Xin, and C. W. Tu, Appl. Phys. Lett. **75**, 501 (1999).
[21] C. Skierbiszewski *et al.*, Phys. Status Solidi B **216**, 135 (1999).
[22] C. Skierbiszewski *et al.*, Appl. Phys. Lett. **76**, 2409 (2000).
[23] A. Lindsay and E. P. O'Reilly, Solid State Commun. **122**, 443 (1999).
[24] M. Hetterich, M. D. Dawson, A. Yu. Egorov, D. Bernklau, and H. Riechert, Appl. Phys. Lett. **76**, 1030 (2000).
[25] P. N. Hai, W. M. Chen, I. A. Buyanova, H. P. Xin, and C. W. Tu, Appl. Phys. Lett. **77**, 1843 (2000).
[26] Y. Zhang, A. Mascarenhas, H. P. Xin, and C. W. Tu, Phys. Rev. B **61**, 7479 (2000).
[27] I. Vurgaftman, J. R. Meyer, and L. R. Ram-Mohan, J. Appl. Phys. **89**, 5815 (2001).
[28] W. Shan *et al.*, Phys. Status Solidi B **223**, 75 (2001).
[29] V. Kytin, V. Duzhko, V. Yu. Timoshenko, J. Rappich, and T. Dittrich, Phys. Status Solidi A **185**, R1 (2001).
[30] C. Hardalov, D. Batovski, and S. Dalakov, Appl. Phys. Lett. **66**, 622 (1995).
[31] A. Fleck, B. J. Robinson, and D. A. Thompson, Appl. Phys. Lett. **78**, 1694 (2001).
[32] R. J. Kaplar, A. R. Arehart, S. A. Ringer, A. A. Allerman, R. M. Sieg, and S. R. Kurtz, Appl. Phys. Lett. **90**, 3405 (2001).